APPLIED MATHEMATICS AND MECHANICS (ENGLISH EDITION)

Numerical investigation of flow over a two-dimensional square cylinder with a synthetic jet generated by a bi-frequency signal[*]

Yiran LU,   Yuan QU,   Jiangsheng WANG,   Jinjun WANG[†]

Fluid Mechanics Key Laboratory of Education Ministry, Beihang University, Beijing 100191, China

Abstract   The flow around a square cylinder with a synthetic jet positioned at the rear surface is numerically investigated with the unsteady Reynolds-averaged Navier-Stokes (URANS) method. Instead of the typical sinusoidal wave, a bi-frequency signal is adopted to generate the synthetic jet. The bi-frequency signal consists of a basic sinusoidal wave and a high-frequency wave. Cases with various amplitudes of the high-frequency component are simulated. It is found that synthetic jets actuated by bi-frequency signals can realize better drag reduction with lower energy consumption when appropriate parameter sets are applied. A new quantity, i.e., the actuation efficiency A_e, is used to evaluate the controlling efficiency. The actuation efficiency A_e reaches its maximum of $0.266\,8$ when the amplitude of the superposed high-frequency signal is 7.5% of the basic signal. The vortex structures and frequency characteristics are subsequently analyzed to investigate the mechanism of the optimization of the bi-frequency signal. When the synthetic jet is actuated by a single-frequency signal with a characteristic velocity of $0.112\,\mathrm{m/s}$, the wake is asymmetrical. The alternative deflection of vortex pairs and the peak at half of the excitation frequency in the power spectral density (PSD) function are detected. In the bi-frequency cases with the same characteristic velocity, the wake gradually turns to be symmetrical with the increase in the amplitude of the high-frequency component. Meanwhile, the deflection of the vortex pairs and the peak at half of the excitation frequency gradually disappear as well.

Key words   synthetic jet, flow control, signal superposition, vortex dynamics

Chinese Library Classification   O358
2010 Mathematics Subject Classification   76F10

Nomenclature

A_0,	amplitude of the basic-frequency component;	C_l,	lift coefficient;
		C_d,	drag coefficient;
A^+,	amplitude ratio between the high-frequency and basic components;	$\boldsymbol{c}_k$,	Fourier mode matrix;
		D,	side length of the square cylinder (mm);
A_e,	actuation efficiency;	$\boldsymbol{F}_n$,	original velocity matrix;

f^+,	frequency ratio between the high-frequency and basic components;	U_{cl},	time-averaged velocity at the centerline (m/s);
f_e,	excitation frequency (Hz);	U_0,	characteristic velocity of the synthetic jets (m/s);
f_0,	natural vortex shedding frequency (Hz);		
L_0,	stroke length of the synthetic jets (mm);	u_0,	streamwise velocity at the jet orifice (m/s);
ν,	kinematic viscosity coefficient;		
Re,	Reynolds number;	u',	streamwise velocity fluctuation (m/s);
t,	time sequence (s);	v',	vertical velocity fluctuation (m/s);
T,	period (s);	w,	width of the slot (mm);
U_∞,	velocity of the incoming flow (m/s);	ω_z,	spanwise vorticity (1/s).

1 Introduction

The flow around a bluff body is a typical fluid mechanics problem in engineering practice and daily life, and is of great value of academic research. The square cylinder, as one of the classical bluff body configurations, has always been considered to be a simplified model of numerous engineering applications. However, the flow around a square cylinder can be quite complex in spite of its simple geometry. A number of studies have been carried out to investigate the characteristics and mechanism of the cylinder wake experimentally or numerically. In the previous literature[1–2], it has been found that with the increment of the Reynolds number, complex phenomena appear successively, e.g., separation, periodic vortex shedding, and three-dimensional (3D) instability. These flow phenomena may lead to unfavorable results including additional drag, unsteady load, vibration induced by vortex and so on, which makes finding the efficient flow control methods significant and necessary for the engineering application.

So far, a variety of methods have been proposed to modify the flow around the square cylinder[3]. Based on whether external energy is needed to actuate the device, the control methods can be divided into two types, i.e., the passive flow control and the active flow control. The passive flow control, with no need of extra energy, manages to achieve the control effect by making 3D geometric modifications to the blunt body, including splitter plate[4], controlling rod[5], small-sized tab[6], roughness[7] and so on. Unlike the passive flow control, the active flow control requires external energy input, including periodic rotation [8], transverse oscillation[9], continuous jets[10], plasma actuators[11] and so on. The synthetic jet[12] is also an important active flow control method, which has been widely investigated during the last two decades for its high efficiency.

The synthetic jet is produced by periodically pushing fluid into the external flow field and entraining fluid back through the orifice or slot of the actuator. Compared with the continuous jets, there is no need of extra fluid to form the synthetic jets, which makes synthetic jet actuators more advantageous in size, weight, and feasibility. It was first used as a laboratory flow control method by Wiltse and Glezer[13] in 1993. Since then, the controlling effect of the synthetic jets and its mechanism have been among the hot topics in fluid mechanics. Amitay et al.[14] applied the synthetic jets to the flow over a circular cylinder at different positions and jet angles, and found that synthetic jets changed the aerodynamic shape of the cylinder and subsequently made modifications to the local flow field around the cylinder. Feng and Wang[15] positioned synthetic jets at the rear stagnation point, and experimentally investigated the vortex structures in the circular cylinder wake. They found out that, for a certain stroke length ratio, with the increment of the synthetic jet excitation frequency, the wake pattern gradually changed from the antisymmetric Karman vortex-shedding mode to the symmetric mode, and thus the wake became fully synchronized by the synthetic jet vortex pairs. Qu et al.[16–17] applied synthetic jets to the square cylinder, and investigated the frequency characteristics and vortex structures in the cylinder wake. The results showed that when the frequency of the synthetic jets was relatively low, i.e., the perturbation of the synthetic jets was weak compared with that of the natural wake vortex shedding, the dominant frequency in the wake was close to the frequency of

the natural vortex shedding. With the increase in the excitation frequency, the synchronization at half and full of the excitation frequency was observed successively. The wake also changed from the natural vortex shedding mode to a mode completely controlled by the synthetic jet vortex pairs.

Improving the control efficiency of synthetic jets is also a research focus in flow control. Luo et al.[18] proposed a new synthetic jet actuator concept, where two adjacent jets were established under the two exit slots and were driven by the motion of the same piezoelectric diagram. The concept was proved to be able to realize evident drag reduction on square cylinder later by Li et al.[19]. Zhang and Wang[20] proposed a novel signal by shortening the blowing cycle of the traditional sinusoidal wave and increasing the peak value of the blowing velocity to generate synthetic jets. They found that the synthetic jets become stronger with increasing the suction duty cycle factor k. The efficiency of this novel signal was verified by them later experimentally on circular cylinder. Lu et al.[21] numerically investigated the synthetic jets actuated by the bi-frequency signal in the quiescent ambient. The novel signal is composed of two sinusoidal waves with different frequencies, i.e., a basic component and a high-frequency component. The frequency of the high-frequency component is an integral of that of the basic component. It was found that when the frequency of the superposed signal was twice of the basic signal, the entrainment of the synthetic jets was enhanced to the maximum. Therefore, in the present study, the bi-frequency signal is utilized to actuate the synthetic jets positioned at a square cylinder as experimentally investigated in Ref. [16]. Comparisons are made between the synthetic jets actuated by the bi-frequency signal and the traditional single-frequency signal to testify the optimum of the bi-frequency signal. The paper is structured as follows. The details of the numerical simulation tools and its validation are given in Section 2. In Section 3, the aerodynamic performance of the cases with bi-frequency and single-frequency signals are described, and the vortex structures and frequency characteristics of the wake are analyzed. Finally, conclusions are given in Section 4.

2 Numerical configuration and validation

All the simulations in the present study are performed with the unsteady Reynolds-averaged Navier-Stokes (URANS) method, along with the open-source software package OpenFOAM. The pressure-velocity coupling is handled by the PIMPLE algorithm. The turbulence model adopted here is the second-moment model developed by Jakirlic and Maduta[22]. Compared with the traditional linear eddy-viscosity model (LEDM), the Reynolds stress model (RSM) can simulate the production of turbulent kinetic energy better, and predict the flow separation more precisely[23]. The two-dimensional (2D) structured grid is utilized. The computational domain and boundary conditions (BCs) are shown in Fig. 1. The origin of the coordinate system is located at the center of the square cylinder, whose side length is $D = 20\,\text{mm}$. The slot is positioned along the centerline of the rear surface of the cylinder, with a width of $w = 1\,\text{mm}$. The inlet boundary is $8D$ upstream of the origin, and a constant velocity BC of $U_\infty = 0.042\,\text{m/s}$ is uniformly applied. The corresponding Reynolds number is $Re = \frac{DU_\infty}{\nu} = 836$, which is the same as Qu et al.[16]. The top and bottom sides of the computational domain are set to be symmetric, $10D$ away from the origin. A zero-gradient BC is applied to the outlet boundary. Since three-dimensionality is not the focus of the present paper, empty BCs are applied to the front and back sides to keep the flow 2D. To simulate the synthetic jets produced by the piston actuator, a cavity is designed inside the square cylinder. The periodic velocity BC is applied to the inner surface of the cavity to simulate the periodic motion of the fluid in the cavity. All the other surfaces of the cylinder and the cavity inside are set to be non-slip.

To make sure that the mesh is adequate for the simulation, grid independence tests are carried out. Three meshes, comprising 44 150, 65 300, and 93 500 elements, are generated, and the baseline case without control is computed with the three meshes, respectively. The time-
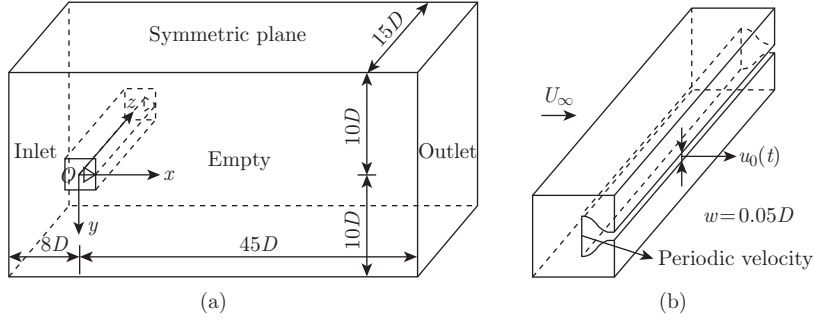
Fig. 1   (a) Illustration of the computational domain; (b) sketch of square cylinder with a cavity inside

averaged drag coefficient C_d, the root mean square of lift coefficient C_{lrms}, and the natural vortex shedding frequency f_0 of the three cases are shown in Table 1. It can be seen that the calculation results of the medium size case and the fine case share little difference. The time-averaged streamwise velocity along the centerline calculated with the three meshes is shown in Fig. 2. The curve of the medium case is quite close to that of the fine case. Therefore, the medium size mesh can be considered to be adequate for the numerical investigation, and is adopted in the following numerical simulation. An adjustable time step algorithm is adopted to make sure that the Courant (CFL) number never exceeds 0.3 in all cases.

Table 1   Comparison of the mean drag coefficient C_d, the root mean square of lift coefficients C_{lrms}, and the vortex shedding frequency f_0 between cases with different mesh sizes

| Mesh size	Cell number	C_d	C_{lrms}	f_0/Hz
Coarse	44 150	1.77	0.68	0.280
Medium	65 300	1.77	0.66	0.285
Fine	93 500	1.77	0.66	0.285

In order to further validate the numerical tools in the present study, particular cases with the same flow conditions in Ref. [16] are computed, and comparisons are made with the experimental results. The flow around the square cylinder controlled by synthetic jets actuated with sinusoidal signals of $f_e/f_0 = 1, 3, 6$ are numerically simulated. The drag coefficients and dominant frequencies of the wake are compared. Considering the drag coefficients measured in the experiments containing the thrust generated by the jets, we additionally perform the simulation in which the synthetic jets with the same exciting parameters are positioned in the quiescent flow, and calculate the thrust created on the cylinder. The comparisons are shown in Table 2 and Fig. 3. According to Qu et al.[16], the synchronization at half and full of the excitation frequency is observed in the cases of $f_e/f_0 = 3$ and $f_e/f_0 = 6$, respectively, which is also captured by our simulation here. The drag reduction with increasing the excitation frequency f_e also shows the same trend with that in the experiments[16]. Therefore, numerical tools are capable for the investigation of the synthetic jet characteristics.

3   Numerical results and discussion

According to the experimental results in Ref. [16], in the case of $f_e/f_0 = 6$ and $L_0 = 72.6\,\mathrm{mm}$, evident drag reduction is achieved, and the synchronization of wake vortex shedding with the synthetic jet is observed. We choose this case as our reference. In the reference case, the single-frequency signal with the excitation frequency $f_e = 6f_0$ is applied. According to the model

Table 2   Comparison of the dominant frequency results obtained by the present study and Qu et al.[16] for particular cases

Case	Dominant frequency	
	Present study	Experiment[16]
No control	$f_0 = 0.285\,\mathrm{Hz}$	$f_0 = 0.3\,\mathrm{Hz}$
$f_\mathrm{e}/f_0 = 1$	$1.02 f_0$	$0.98 f_0$
$f_\mathrm{e}/f_0 = 3$	$1.50 f_0$	$1.52 f_0$
$f_\mathrm{e}/f_0 = 6$	$6.01 f_0$	$5.96 f_0$
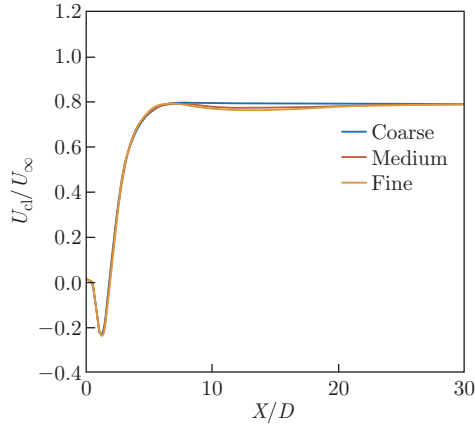
Fig. 2   Time-averaged streamwise velocity along the centerline calculated with different mesh sizes (color online)
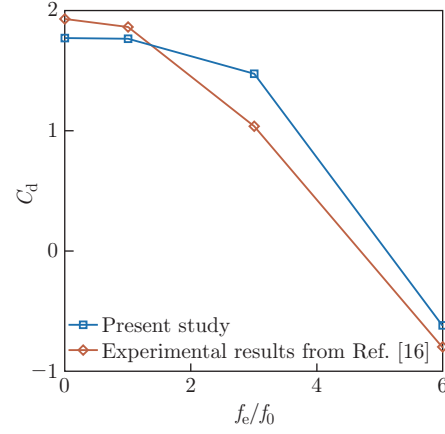
Fig. 3   Comparison of the mean drag coefficient C_d between the present study and the experimental results from Ref. [16] (color online)

adopted by Glezer et al.[24], the characteristic velocity of the synthetic jet is defined as

$$U_0 = \frac{1}{T} \int_0^{T/2} u_0(t)\mathrm{d}t, \tag{1}$$

$$L_0 = U_0/f_\mathrm{e}, \tag{2}$$

where $u_0(t)$ is the instant streamwise velocity at the exit. Therefore, the characteristic velocity U_0 in the single-frequency reference case is $U_0 = 0.124\,\mathrm{m/s}$. The bi-frequency signal to actuate the synthetic jets is defined as

$$u_0(t) = A_0(\sin(2\pi f_\mathrm{basic}t) + A^+ \sin(2\pi f_\mathrm{high}t)). \tag{3}$$

According to our previous research[21], when $f^+ = f_\mathrm{high}/f_\mathrm{basic} = 2$, the entrainment of the synthetic jets enhances the most. Therefore, the frequency ratio f^+ in the present study is kept constant at $f^+ = 2$. The signal adopted in the present study is thus defined as

$$u_0(t) = A_0(\sin(12\pi f_0 t) + A^+ \sin(24\pi f_0 t)). \tag{4}$$

The waveshapes of the typical bi-frequency signal identified in Eq. (4) are shown in Fig. 4.
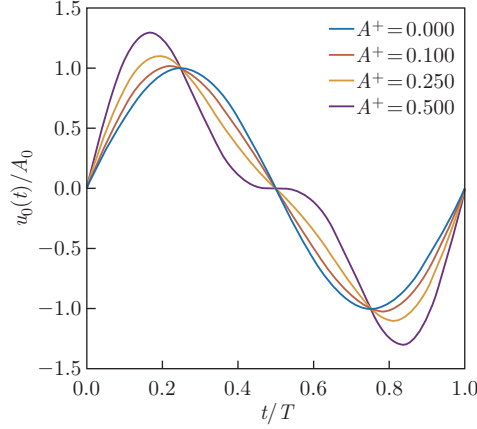
Fig. 4 Waveshapes of the bi-frequency signal identified in Eq. (4) (color online)

Since the frequency of the superposed signal is twice of that of the basic signal, the superposition does not make any change to the characteristic velocity of the synthetic jets U_0. The bi-frequency signal can be uniquely identified by the characteristic velocity U_0 and the amplitude ratio between the high-frequency component and the basic component A^+. According to Ref. [21], the superposition of the high-frequency component can strengthen the synthetic jets without increasing the characteristic velocity. Thus, we mainly focused on the synthetic jets actuated by the bi-frequency signal with lower characteristic velocity U_0 in the present paper. Synthetic jets with 100%, 90%, 80%, and 70% of the characteristic velocity U_0 in the reference case are investigated. The corresponding characteristic velocities are $U_0 = 0.124 \, \text{m/s}$, $0.112 \, \text{m/s}$, $0.099 \, \text{m/s}$, and $0.087 \, \text{m/s}$, respectively. The actuating parameters f_0, A_0, and A^+ and the characteristic velocity U_0 of all the cases are listed in Table 3. For each characteristic velocity, cases with varying amplitude ratio A^+ are simulated. The statistical characteristics of the flow field are analyzed first, and the vortex dynamics are investigated subsequently to explain the mechanism of the optimization case in detail.

Table 3 Actuating parameters f_0, A_0, and A^+ and the characteristic velocity U_0 of all the cases

Case No.	f_0/Hz	A_0	A^+	U_0/(m/s)
1	0.285	0.390	0.000	0.124
2	0.285	0.390	0.050	0.124
3	0.285	0.390	0.100	0.124
4	0.285	0.390	0.200	0.124
5	0.285	0.351	0.000	0.112
6	0.285	0.351	0.050	0.112
7	0.285	0.351	0.075	0.112
8	0.285	0.351	0.100	0.112
9	0.285	0.351	0.150	0.112
10	0.285	0.351	0.200	0.112
11	0.285	0.312	0.000	0.099
12	0.285	0.312	0.100	0.099
13	0.285	0.312	0.125	0.099
14	0.285	0.312	0.150	0.099
15	0.285	0.312	0.175	0.099
16	0.285	0.312	0.200	0.099
17	0.285	0.273	0.000	0.087
18	0.285	0.273	0.200	0.087
19	0.285	0.273	0.350	0.087
20	0.285	0.273	0.400	0.087
21	0.285	0.273	0.500	0.087

3.1 Statistical characteristics of flow field

The control effects, i.e., the drag coefficient reduction $|\Delta C_{\mathrm{d}}|$ and the fluctuation of the lift coefficient C_{lrms}, of the synthetic jets are presented in Figs. 5(a) and 5(b), respectively. The net drag reduction $|\Delta C_{\mathrm{d}}|$ is compared with the case without control, where $C_{\mathrm{d}} = 1.77$. As shown in Fig. 5(a), all the curves, except the one with $U_0 = 0.124 \,\mathrm{m/s}$, share the same variation trend that the drag reduction first increases with the amplitude ratio, reaches the maximum, and then decreases, while the curve with $U_0 = 0.124 \,\mathrm{m/s}$ monotonously decreases with the amplitude ratio. The largest drag reduction is achieved at $U_0 = 0.112 \,\mathrm{m/s}$ and $A^+ = 0.075$, where the flow control effect is realized with lower energy consumption than that in the single-frequency case at $U_0 = 0.124 \,\mathrm{m/s}$. When the characteristic velocity further decreases, the drag reduction effect gradually diminishes. Different from the drag coefficient, the fluctuations of the lift coefficient C_{lrms} monotonously decrease firstly, and reach a plateau for all characteristic velocities investigated. In addition, the plateaus of C_{lrms} in all cases are approximately at the same level. Since only cases with $U_0 = 0.112 \,\mathrm{m/s}$ are able to achieve better drag reduction than the reference case with $U_0 = 0.124$ m/s, the following investigation mainly focuses on the cases with $U_0 = 0.112 \,\mathrm{m/s}$ and the single-frequency case with $U_0 = 0.124 \,\mathrm{m/s}$. In order to evaluate the controlling efficiency of the synthetic jets with energy consumption taken into consideration, we adopt a new physical quantity, i.e., actuation efficiency A_{e}, as follows:

$$A_{\mathrm{e}} = \frac{\frac{1}{2}|\Delta C_{\mathrm{d}}|S U_\infty^3 + \frac{1}{2T}S_{\mathrm{jet}}U_\infty \int_0^{T/2} u^2(t)\mathrm{d}t}{\frac{1}{2T}S_{\mathrm{jet}} \int_0^{T/2} u^3(t)\mathrm{d}t}, \tag{5}$$

where $|\Delta C_{\mathrm{d}}|$ is the net drag reduction compared with the case without control, and S and S_{jet} are the areas of the rear surface of the cylinder and the slot, respectively. The actuation efficiency is defined as the ratio between the saved energy and the energy consumed to generate the synthetic jets. The energy saving can be attributed to two parts, i.e., the drag reduction and the thrust generated by the synthetic jets. The actuation efficiencies for cases with $U_0 = 0.112 \,\mathrm{m/s}$ and $0.124 \,\mathrm{m/s}$ are shown in Fig. 5(c). With energy consumption taken into account, the actuation efficiency of bi-frequency cases with lower characteristic velocity $U_0 = 0.112 \,\mathrm{m/s}$ is significantly higher than that of the single-frequency with $U_0 = 0.124 \,\mathrm{m/s}$. The highest actuation efficiency is obtained at $U_0 = 0.112 \,\mathrm{m/s}$ and $A^+ = 0.075$, where the best drag reduction is achieved as well. The optimal actuation efficiency A_{e} is 0.266 8, which is 21% higher than that in the reference case ($A_{\mathrm{e}} = 0.22$).
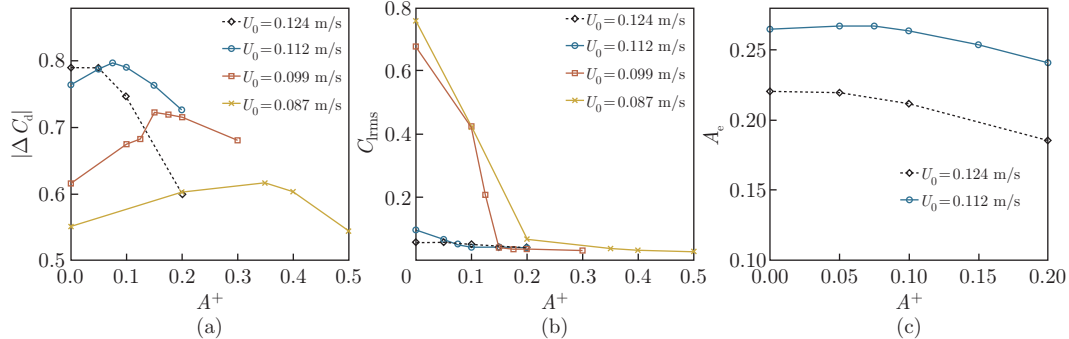

Fig. 5 Variations of (a) drag reduction coefficient $|\Delta C_{\mathrm{d}}|$, (b) root mean square of lift coefficient fluctuation C_{lrms}, and (c) actuation efficiency for different characteristic velocities with varying amplitude ratio A^+ (color online)

In order to investigate the drag reduction mechanism of the synthetic jets generated by the bi-frequency signal, the velocity field is analyzed. The distributions of the streamwise velocity fluctuation and the vertical velocity fluctuation sampled at two different streamwise

locations are shown in Fig. 6. The application of synthetic jets significantly suppresses the velocity fluctuations in both directions. However, compared with the reference case, the level of velocity fluctuations in the case with $U_0 = 0.112\,\mathrm{m/s}$ and $A^+ = 0.000$ is obviously higher. With high-frequency signal superposed, the fluctuations gradually decrease with the increasing high-frequency component amplitude. In the case with the amplitude ratio $A^+ = 0.100$, the fluctuations basically drop to the same level as the reference case. It means that, the superposition of the high-frequency wave manages to enhance the synthetic jets, similar to that achieved by increasing the characteristic velocity U_0. The distribution of the Reynolds stress presented in Fig. 7 shows the similar variation trend, which corroborates the enhancement due to the bi-frequency signal and corresponds to the subsequential drag reduction mentioned in Fig. 5(a).
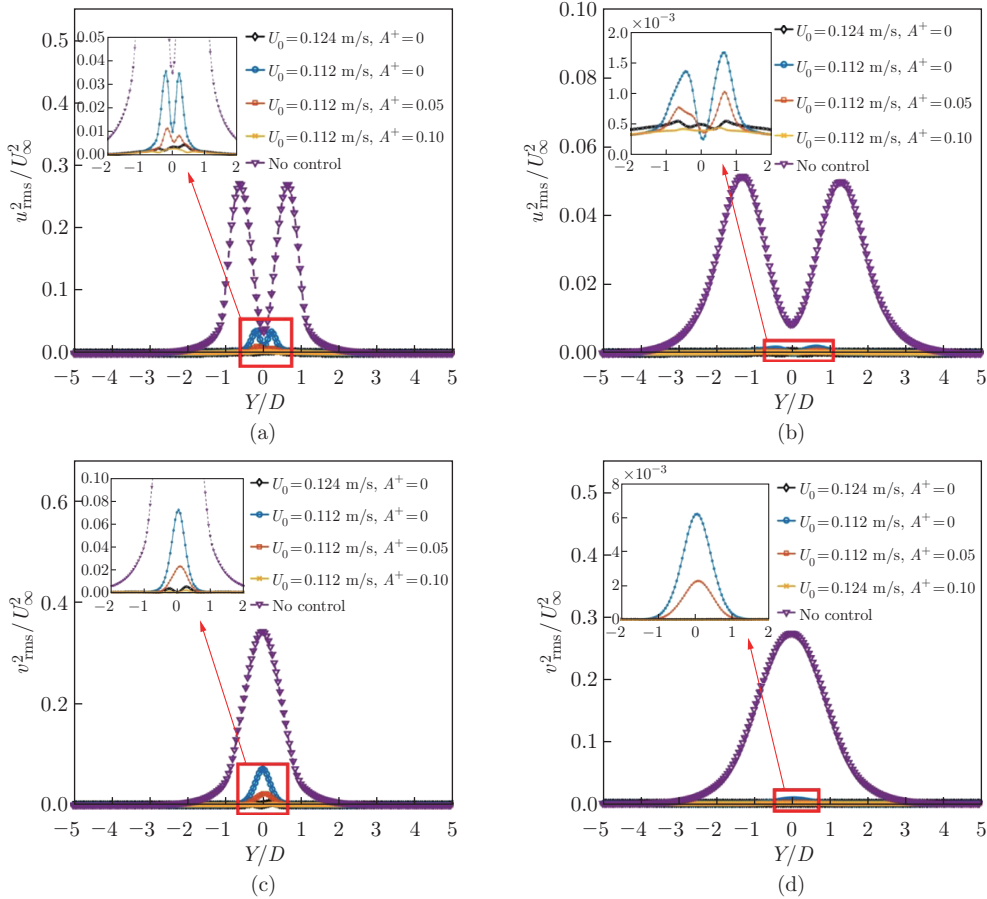
Fig. 6 Distributions of the streamwise velocity fluctuation (a, b) and the vertical velocity fluctuation (c, d) along the vertical direction. (a, c) are sampled at $X/D = 2$, and (b, d) are sampled at $X/D = 5$ (color online)

3.2 Wake vortex dynamics

The evolutions of the vortex structures and the frequency characteristics are investigated in this part to further explain how the bi-frequency signal enhances the synthetic jets and optimizes the control efficiency. In light of the aerodynamic performance shown in Subsection 3.1, only the results from the cases with $U_0 = 0.112\,\mathrm{m/s}$ and the single-frequency case with $U_0 = 0.124\,\mathrm{m/s}$ are presented here. The single-frequency signal with $f_e = 6f_0$ and $U_0 = 0.124\,\mathrm{m/s}$ is utilized as the reference case. The contour of the phase-averaged vorticity is shown in Fig. 8. The vorticity is normalized with U_∞ and D. It can be seen that the wake is symmetrical and the vortex pairs induced by the synthetic jets travel downstream along the centerline, which indicates the
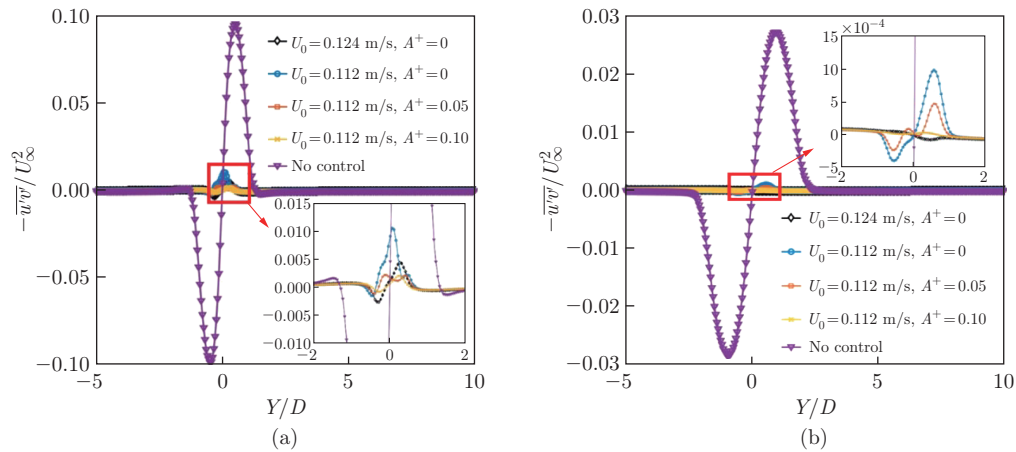
Fig. 7 Distributions of the Reynolds shear stress along the vertical direction at (a) $X/D = 2$ and (b) $X/D = 5$ (color online)

wake, is fully dominated by the synthetic jets. It is verified by the time history and power spectral density function in Fig. 9. The time history and power spectral density (PSD) function are calculated with the streamwise velocity sampled at the point $(x, y) = (1D, 0.5D)$ near the position where the fluctuation of the streamwise velocity u_{rms} reaches its maximum in the upper shear layer. The time history is highly periodic, and the dominant frequency of $6f_0$ is detected in the PSD function, which is exactly the excitation frequency f_{e}. Therefore, it can be corroborated that the so-called lock-in phenomenon takes place.

Considering the PSD calculated with the fast Fourier transformation (FFT) method can only reflect the frequency characteristics at a separated point, the Fourier mode decomposition
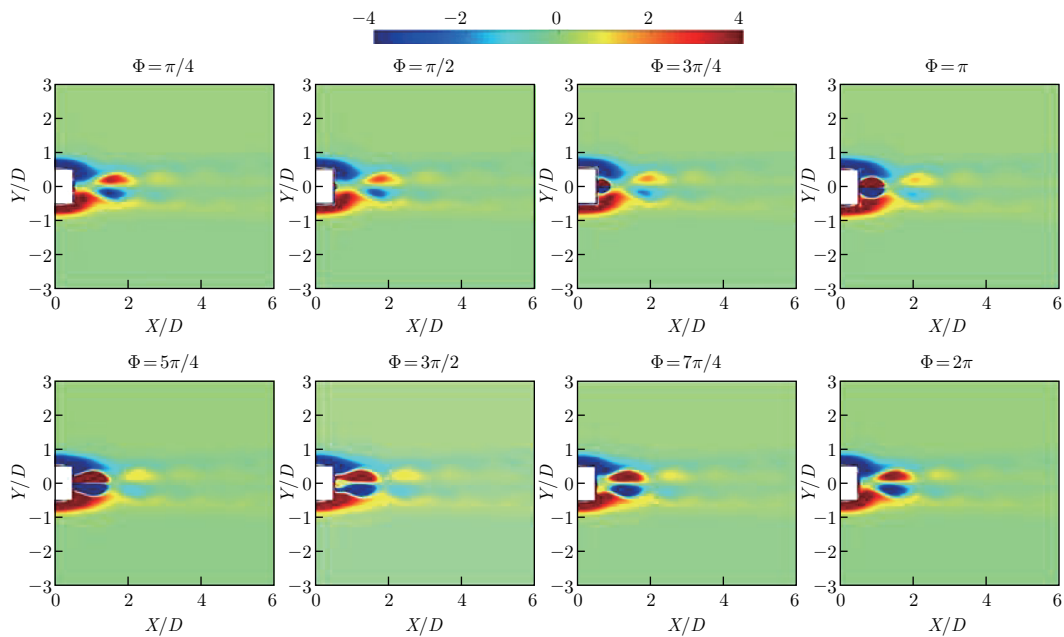
Fig. 8 Evolution of the phase-averaged spanwise vorticity $\omega_z D/U_\infty$ for the reference case with $f_{\mathrm{e}} = 6f_0$ and $U_0 = 0.124\,\mathrm{m/s}$ (color online)
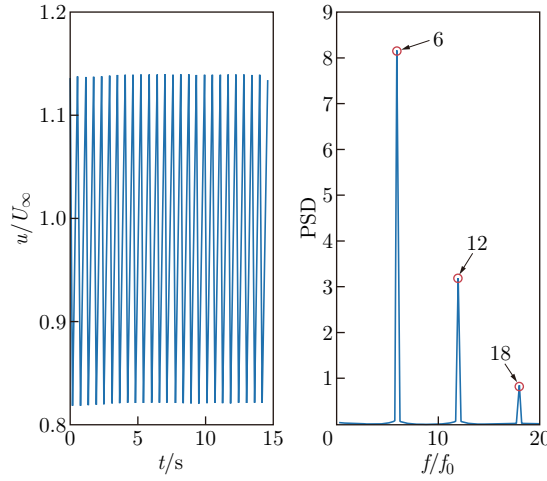
Fig. 9   Time history and power spectral density function of the streamwise velocity at $(1D, 0.5D)$ for the reference case with $f_e = 6f_0$ and $U_0 = 0.124\,\mathrm{m/s}$ (color online)

(FMD) method proposed by Ma et al.[25] is also utilized to analyze the component of each peak value in the whole flow field. The FMD method is an algorithm based on the single-point discrete Fourier transformation (DFT). By applying a single-point discrete Fourier transformation to every velocity sequence inside the original velocity matrix achieved by particle image velocimetry (PIV) experiments or numerical simulation, a mode matrix c_k is achieved as follows:

$$c_k = \frac{1}{N} \sum_{n=0}^{N} F_n \mathrm{e}^{-\mathrm{i}\left(\frac{2\pi k}{N}\right)n},\tag{6}$$

where N is the total sampling number of image pairs, and F_n is the original velocity matrix. The global PSD (P_k) is further defined as

$$P_k = \left\|\frac{2N|c_k|^2}{\pi f_s}\right\|,\tag{7}$$

where $\|\cdot\|$ is the Frobenius norm, and f_s is the sampling frequency. Based on the global power spectrum, the dynamic mode along with its amplitude according to the individual characteristic frequency can be effectively extracted. According to Ma et al.[25], the FMD method can present the coherent structures at individual frequencies, which makes its results well defined with regard to their physical meaning. The normalized global PSD function is presented in Fig. 10, normalized with the maximum value of the curve. The global PSD is concentrated at the same frequencies as the PSD calculated at the single point, which verifies the existence of the synchronization phenomenon.

When the synthetic jets are still generated by single-frequency signals, but with a lower characteristic velocity $U_0 = 0.112\,\mathrm{m/s}$, the evolution of the vortex structures shows some difference. In Fig. 11, the vortex pairs no longer travel downstream along the centerline, but slightly deflect upward and downward alternatively, and the wake shows the asymmetric characteristic. Although the dominant frequency is still at $f = 6f_0$, a new characteristic frequency peak at $f/f_0 = 3$ arises in the normalized PSD function in Fig. 12. The newly arising peak at $f/f_0 = 3$ corresponds to the alternate deflection of the vortex pairs shown in Fig. 11. According to Ref. [16], when synthetic jets are strong enough to fully control the wake, the
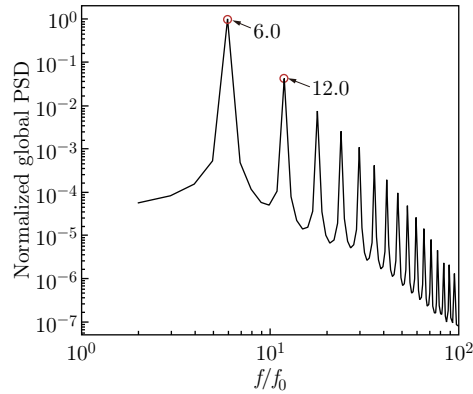
Fig. 10   Normalized global power spectrum for the reference case with $f_e = 6f_0$ and $U_0 = 0.124\,\mathrm{m/s}$
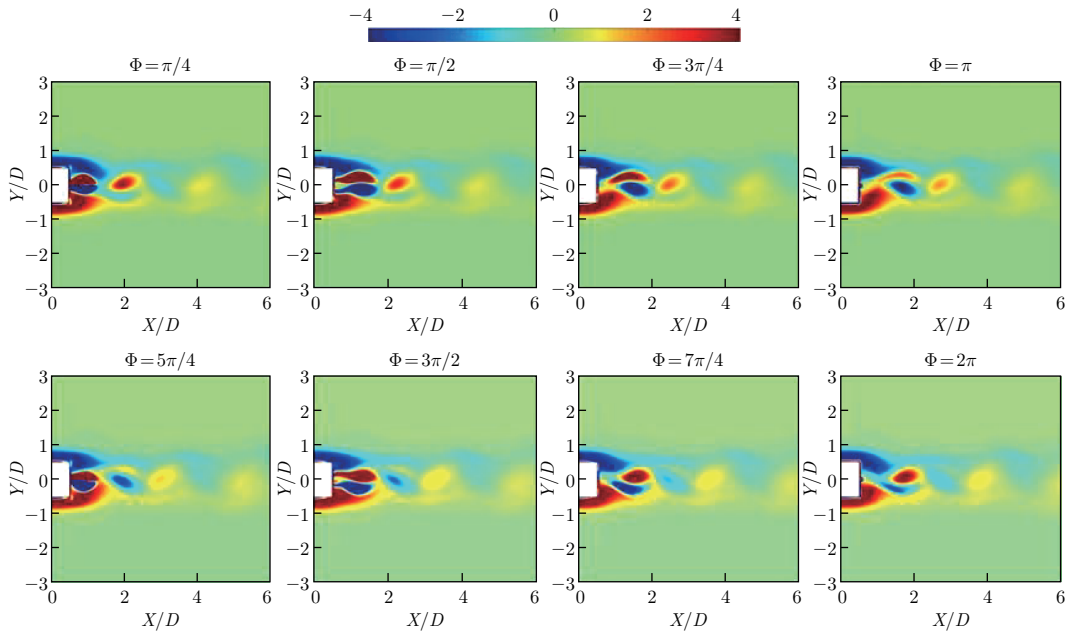

Fig. 11   Evolutions of the phase-averaged spanwise vorticity $\omega_z D/U_\infty$ for the single-frequency case with $f_e = 6f_0$ and $U_0 = 0.112\,\mathrm{m/s}$ (color online)
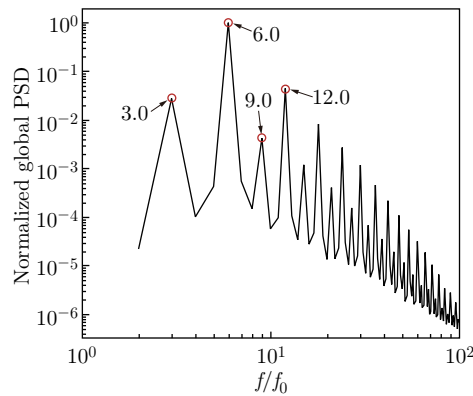

Fig. 12   Normalized global power spectrum for the single-frequency case with $f_e = 6f_0$ and $U_0 = 0.112\,\mathrm{m/s}$

peaks below the excitation frequency should not be observed in the PSD function, as shown in Fig. 10. Therefore, the occurrence of the peak at $f/f_0 = 3$ indicates the deficiency of the synthetic jets due to the decrease in the characteristic velocity. In order to further investigate the component at $f/f_0 = 3$, the amplitude value of the Fourier mode calculated by the FMD method at $f/f_0 = 3$ is shown in Fig. 13. The amplitude calculated based on the streamwise velocity presents a symmetrical property, distributed near the centerline. While the amplitude value of the vertical velocity concentrates at a single peak region away from the cylinder.
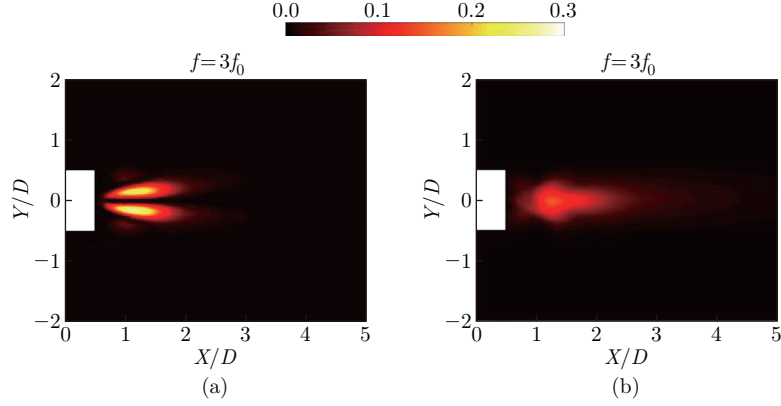
Fig. 13   Amplitude of the Fourier mode at $f/f_0 = 3$ based on (a) the streamwise velocity and (b) the vertical velocity for the single-frequency case with $f_e = 6f_0$ and $U_0 = 0.112\,\mathrm{m/s}$ (color online)

When the bi-frequency signal instead of the single-frequency sinusoidal wave is used to generate the synthetic jets, although the characteristic velocity keeps the same, the vortex structures are different. The evolution of the phase-averaged vorticity in the case with $U_0 = 0.112\,\mathrm{m/s}$ and $A^+ = 0.050$ is shown in Fig. 14. The alternative deflection is not so evident as in the previous
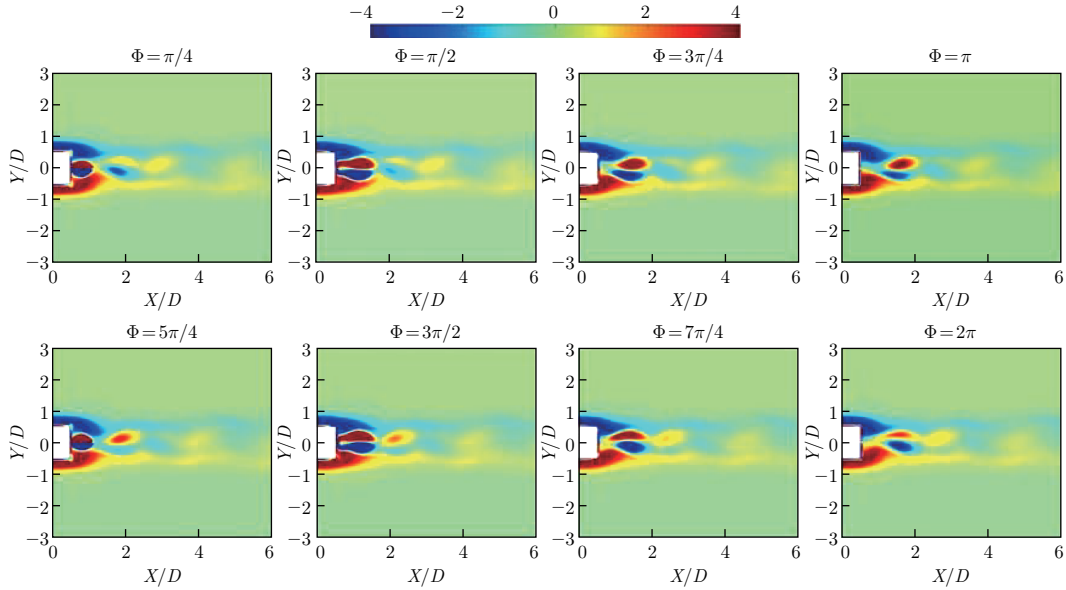

Fig. 14   Evolution of the phase-averaged spanwise vorticity $\omega_z D/U_\infty$ for the bi-frequency case with $f_{\mathrm{basic}} = 6f_0$, $f_{\mathrm{high}} = 12f_0$, $A^+ = 0.050$, and $U_0 = 0.112\,\mathrm{m/s}$ (color online)

case, though it still can be observed. The peak at $f/f_0 = 3$ in the global PSD function can be detected as well in Fig. 15. However, in this case, the peak value at $3f_0$ decreases to some extent. The amplitude values of the Fourier mode calculated with the FMD method at $f/f_0 = 3$ are shown in Fig. 16. The distribution is similar to that in the single-frequency case with $U_0 = 0.112\,\mathrm{m/s}$. However, the amplitudes are significantly attenuated, indicating a weakened intensity of the coherent structures at $f/f_0 = 3$, which corresponds to the alternative deflection. Since the alternative deflection occurs when the synthetic jets are not strong enough, the attenuation of the structures at $f/f_0 = 3$ also verifies the result mentioned in Subsection 3.1 that the superposition of the high-frequency signal manages to enhance the synthetic jets.
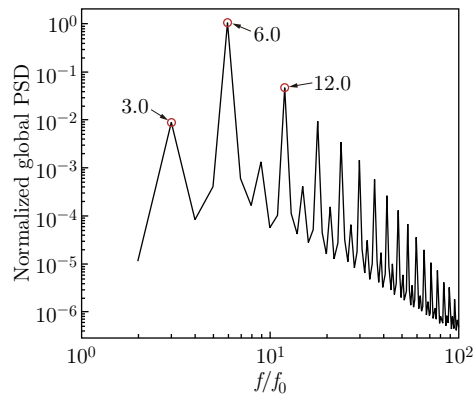

Fig. 15   Normalized global power spectrum for the bi-frequency cases with $f_{\mathrm{basic}} = 6f_0$, $f_{\mathrm{high}} = 12f_0$, $A^+ = 0.050$, and $U_0 = 0.112\,\mathrm{m/s}$
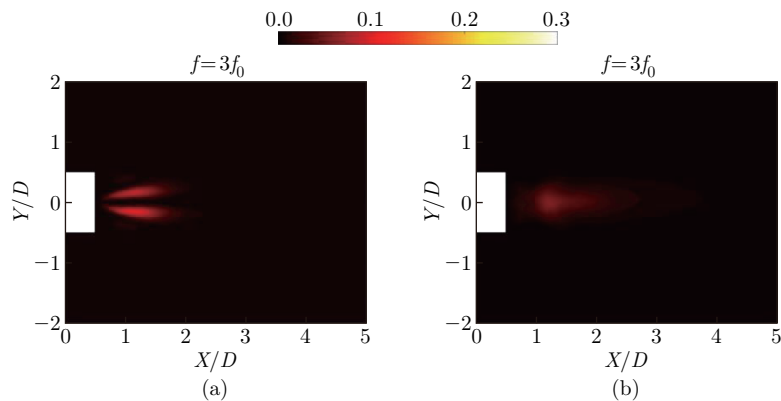

Fig. 16   Amplitude of the Fourier mode at the characteristic frequency $f/f_0 = 3$ based on (a) the streamwise velocity and (b) the vertical velocity for the bi-frequency case with $f_{\mathrm{basic}} = 6f_0$, $f_{\mathrm{high}} = 12f_0$, $A^+ = 0.050$, and $U_0 = 0.112\,\mathrm{m/s}$ (color online)

When the amplitude ratio of the superposed high-frequency signal increases to $A^+ = 0.100$, the evolution of the vorticity presented in Fig. 17 is quite similar to that in the reference case. The vortex pairs induced by the synthetic jets move downstream along the centerline, and the wake is basically symmetrical again. The peak at $f/f_0 = 3$ is no longer observed in the normalized PSD in Fig. 18. When the amplitude ratio A^+ is further increased, the vortex structures and the frequency characteristics in the wake are no more altered, and thus the results of the cases with higher amplitude ratios are not presented in this paper.
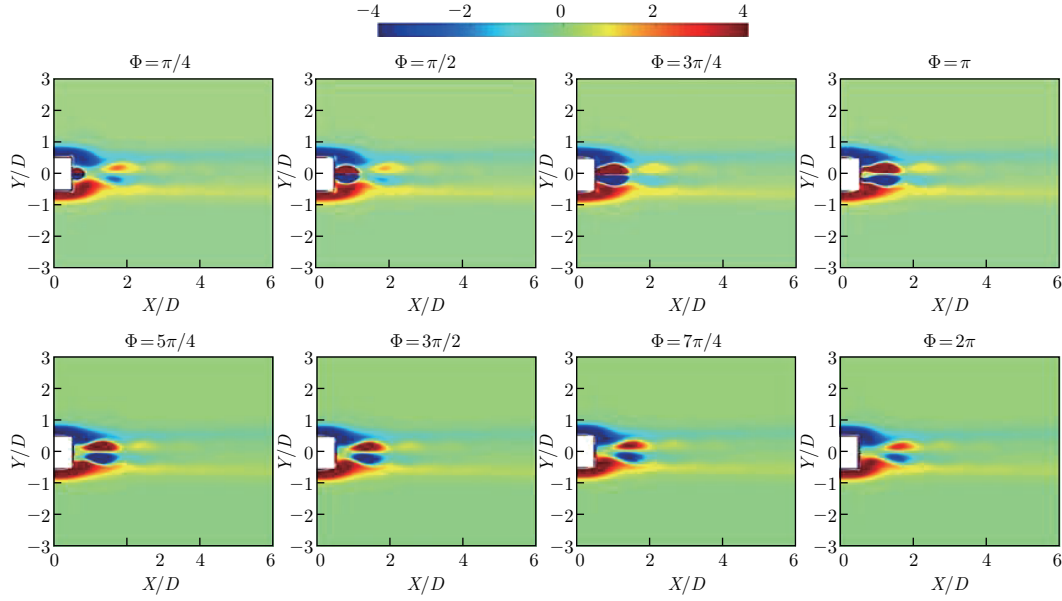
Fig. 17 Evolutions of the phase-averaged spanwise vorticity $\omega_z D/U_\infty$ for the bi-frequency case with $f_{\text{basic}} = 6f_0$, $f_{\text{high}} = 12f_0$, $A^+ = 0.100$, and $U_0 = 0.112\,\text{m/s}$ (color online)
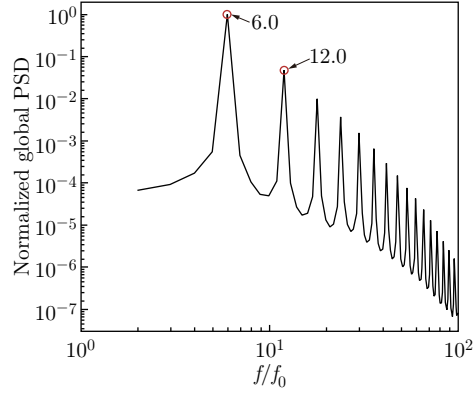

Fig. 18 Normalized global power spectrum for the bi-frequency case with $f_{\text{basic}} = 6f_0$, $f_{\text{high}} = 12f_0$, $A^+ = 0.100$, and $U_0 = 0.112\,\text{m/s}$

4 Conclusions

In the present study, the flow control over a square cylinder with a synthetic jet generated by bi-frequency signals is numerically investigated. The conclusions can be summarized as follows.

(i) Better drag reduction can be achieved with lower energy consumption when the bi-frequency signal is adopted to generate the synthetic jets. Optimal flow control is realized in the case with $A^+ = 0.075$ and $U_0 = 0.112\,\text{m/s}$, where A_e is $0.266\,8$, which is 21% higher than A_e (= 0.22) in the single-frequency case with $U_0 = 0.124\,\text{m/s}$.

(ii) The mechanism of the optimization of the bi-frequency synthetic jets is revealed by analyzing the vortex structures and the frequency characteristics. When the synthetic jet is actuated by a single-frequency signal with the characteristic velocity $U_0 = 0.112\,\text{m/s}$, the wake is asymmetrical. The alternative deflection of vortex pairs induced by the synthetic jets and the

peak at half of the excitation frequency in the PSD function are detected due to the deficiency of the synthetic jets. With the high-frequency signal superposed, the synthetic jets get enhanced without increasing the characteristic velocity. The phenomena including the deflection of the vortex pairs and the peak at half of the excitation frequency gradually disappear with increasing the amplitude of the superposed high-frequency signal. When the amplitude ratio reaches $A^+ = 0.100$, the wake becomes completely dominated by the synthetic jets, and the flow field is basically consistent with that of the single-frequency case with $U_0 = 0.124\,\text{m/s}$.

References

[1] SOHANKAR, A., NORBERG, C., and DAVIDSON, L. Low-Reynolds-number flow around a square cylinder at incidence: study of blockage, onset of vortex shedding and outlet boundary condition. *Internation Journal for Numerical Methods in Fluids*, **26**, 39–56 (1998)

[2] CHOI, H., JEON, W. P., and KIM, J. Control of flow over a bluff body. *Annual Review of Fluid Mechanics*, **40**, 113–139 (2008)

[3] WANG, J. J. and FENG, L. H. *Flow Control Techniques and Applications*, Cambridge University Press, Cambridge (2018)

[4] ALI, M. S. M., DOOLAN, C. J., and WHEATLEY, V. Control of flow over a bluff body. *Physics of Fluids*, **23**(3), 033602 (2011)

[5] ZHANG, P. F., WANG, J. J., LU, S. F., and MI, J. Aerodynamic characteristics of a square cylinder with a rod in a staggered arrangement. *Eperimets in Fluids*, **38**, 494–502 (2005)

[6] PARK, H., LEE, D., JEON, W. P., HAHN, S., KIM, J., KIM, J., and CHOI, J. Drag reduction in flow over a two-dimensional bluff body with a blunt trailing edge using a new passive device. *Journal of Fluid Mechanics*, **563**, 389–414 (2006)

[7] VAN HINSBERG, N. P., SCHEWE, G., and JACOBS, M. Experimental investigation on the combined effects of surface roughness and corner radius for square cylinders at high Reynolds numbers up to 10^7. *Journal of Wind Engineering and Industrial Aerodynamics*, **173**, 14–27 (2018)

[8] MITTAL, S. and KUMAR, B. Drag reduction in flow over a two-dimensional bluff body with a blunt trailing edge using a new passive device. *Journal of Fluid Mechanics*, **476**, 303–334 (2003)

[9] CHAUHAN, M. K., DUTTA, S., GANDHI, B. K., and MORE, B. S. Experimental investigation of flow over a transversely oscillating square cylinder at intermediate Reynolds number. *Journal of Fluids Engineering-Transactions of the ASME*, **138**(5), 051105 (2016)

[10] AKANSU, Y. E., FIRT, E., and HACIALIOGULLARI, M. Reduction of fluid forces acting on a square prism using a planar jet. *Experimental Thermal and Fluid Science*, **86**, 11–22 (2017)

[11] ANZAI, Y., FUKAGATA, K., MELIGA, P., BOUJO, E., and GALLAIRE, F. Numerical simulation and sensitivity analysis of a low-Reynolds-number flow around a square cylinder controlled using plasma actuators. *Physical Review Fluids*, **2**(4), 043901 (2017)

[12] ZHANG, P. F., WANG, J. J., and FENG, L. H. Review of zero-net-mass-flux jet and its application in separation flow control. *Science in China Series E: Technological Sciences*, **51**, 1315–1344 (2008)

[13] WILTSE, J. and GLEZER, A. Manipulation of free shear flows using piezoelectric actuators. *Journal of Fluid Mechanics*, **249**, 261–285 (1993)

[14] AMITAY, M., HONOHAN, A. M., TRAUTMAN, M., and GLEZER, A. Modification of the aerodynamic characteristics of bluff bodies using fluidic actuators. *28th Fluid Dynamics Conference*, AIAA, Snowmass Village (1997)

[15] FENG, L. H. and WANG, J. J. Circular cylinder vortex-synchronization control with a synthetic jet positioned at the rear stagnation point. *Journal of Fluid Mechanics*, **662**, 232–259 (2010)

[16] QU, Y., WANG, J. J., SUN, M., FENG, L. H., PAN, C., GAO, Q., and HE, G. S. Circular cylinder vortex-synchronization control with a synthetic jet positioned at the rear stagnation point. *Journal of Fluid Mechanics*, **812**, 940–965 (2017)

[17] QU, Y., WANG, J. J., FENG, L. H., and HE, X. Effect of excitation frequency on flow characteristics around a square cylinder with a synthetic jet positioned at front surface. *Journal of Fluid Mechanics*, **880**, 764–798 (2019)

[18] LUO, Z. B., XIA, Z. X., and LIU, B. New generation of synthetic jet actuators. *AIAA Journal*, **44**(10), 2418–2420 (2006)

[19] LI, S. Q., LUO, Z. B., DENG, X., PENG, W. Q., and LIU, Z. Y. Experimental investigation on active control of flow around a finite-length square cylinder using dual synthetic jet. *Journal of Wind Engineering and Industrial Aerodynamics*, **210**, 104519 (2021)

[20] ZHANG, P. F. and WANG, J. J. Novel signal wave pattern for efficient synthetic jet generation. *AIAA Journal*, **45**(5), 1058–1065 (2007)

[21] LU, Y. R., WANG, J. S., and WANG, J. J. Numerical investigation of efficient synthetic jets generated by multiple-frequency actuating signals. *Acta Mechanica Sinica*, **38**, 321177 (2022)

[22] JAKIRLIC, S. and MADUTA, R. Extending the bounds of 'steady' RANS closures: toward an instability-sensitive Reynolds stress model. *International Journal of Heat and Fluid Flow*, **51**, 175–194 (2015)

[23] PALKIN, E., MULLYADZGANOV, R., HADZIABDIC, M., and HANJALIC, K. Scrutinizing URANS in shedding flows: the case of cylinder in cross-flow in the subcritical regime. *Flow Turbulence and Combustion*, **97**(4), 1017–1046 (2016)

[24] GLEZER, A., AMITAY, M., and HONOHAN, A. M. Aspects of low and high frequency actuation for aerodynamic flow control. *AIAA Journal*, **43**(7), 1501–1511 (2005)

[25] MA, L. Q., FENG, L. H., PAN, C., GAO, Q., and WANG, J. J. Fourier mode decomposition of PIV data. *Science China*: *Technological Science*, **58**(11), 1935–1948 (2015)